Preparation and Characterization and Dielectric Properties of (Ba0.95Ca0.05) TiO3 Ceramic Material

G.M. Rashwan
Physics Department, Faculty of Science, South Valley University, Qena 83523, Egypt.,
masoud.mostafa@sci.svu.edu.eg

A.A Ebnalwaleda
Egypt nanotechnology center (EGNC), Cairo University, sheik Zayed campus 12588 Giza, Egypt.,
masoud.mostafa@sci.svu.edu.eg

M.K. Gerges
Physics Department, Faculty of Science, South Valley University, Qena 83523, Egypt.,
masoud.mostafa@sci.svu.edu.eg

M. Mostafa
Physics Department, Faculty of Science, South Valley University, Qena 83523, Egypt. \\ Physics Department, College of Science, Jouf University, Sakaka, Saudi Arabia., masoud.mostafa@sci.svu.edu.eg

Preparation and Characterization and Dielectric Properties of (Ba0.95Ca0.05) TiO3 Ceramic Material

G.M. Rashwan [1] *, A.A Ebnalwaleda,* [3] *, M.K. Gerges*[1] *, M. Mostafa* [12*]

[1] Physics Department, Faculty of Science, South Valley University, Qena 83523, Egypt.
[2] Physics Department, College of Science, Jouf University, Sakaka, Saudi Arabia.
[3] Egypt nanotechnology center (EGNC), Cairo University, sheik Zayed campus 12588 Giza, Egypt.

Abstract: (Ba0.95 Ca0.05)TiO3 ceramic was prepared by solid-state reaction method for different calcination temperatures 1100°C, 1150°C, and 1200°C. X-ray Diffraction (XRD) analysis was performed, it shows that the crystallization starts to form at 1200°C. Sintering was carried out at 1400°C for 3 hours. The sample was characterized by transmission electron microscopy (TEM), scan electron microscopy (SEM), and UV-Visible spectrophotometer. Dielectric properties of this sample were measured in the temperature range 25oC - 140oC, which demonstrates that the maximum dielectric constant (ε) =1982. Rietveld refinement analysis for the XRD pattern is performed, which indicated that Ca-ions enter the tetragonal unit cell and replace Ba-ion and maintain the perovskite tetragonal structure.

Keywords: Ferroelectric, Ceramic, BaCaTiO3, Dielectric properties, Structure.

1 Introduction

Ferroelectric materials have a wide-ranging of applications for their excellent dielectric, piezoelectric and ferroelectric properties[1], ceramic materials had attracted large interest for several practical applications such as oscillators, delay lines, steerable antennas, parametric amplifiers, capacitors, varactors, resonators, voltage-controlled oscillators, tunable filters and phase shifters [2]–[8] due to their superior electrically tunable dielectric properties in tunable microwave devices.

Barium titanate based lead-free ferroelectric or piezoelectric materials are in great need due to their eco-friendly nature these materials have several applications such as sensors, transducers, and actuators, etc.[9]. Barium titanate $BaTiO_3$ is an ABO_3 perovskite-type structure and the oxygen ions plus the barium ions form a cubic lattice. The titanium atoms reside in octahedral interstitial positions surrounded by six oxygen ions. Because of the large size of the Ba ions, titanium has slightly deviated from the center [10]. Barium calcium titanate (BCT) has a larger piezoelectric response than pure BT [11]. Ca doped $BaTiO_3$ ($Ba_{1-x}Ca_xTiO_3$, BCT) crystals are one of the most famous potential candidates for the lead-free electro-optic modulators and memory devices. Microstructure and

conventional solid-state reaction technique have been Described by several authors. It has been found that Ca^{2+} replaces Ba^{2+} in $BaTiO_3$ to form tetragonal BCT solid solutions when x is less than 0.23 [12], and calcium acts as a reduction inhibitor in $BaTiO_3$ and reduces the possibility of creation of the undesirable hexagonal phase. But there are few reports on the effect of electric field on dielectric properties [13]. BaTiO3 doped Ca2+ ions in the range of (0.05–0.3 mol.%) were considered a promising lead-free material with outstanding piezoelectric properties due to orthorhombic tetragonal coexistence of BT and CT phases and from a morphotropic phase boundary (MPB) at room temperature with very low dielectric loss values in a ferroelectric phase [14].

This study is aimed to study the physical properties of $(Ba_{0.95}Ca_{0.05})TiO_3$ nanoparticles prepared by the solid-state reaction method. The structural, optical, and dielectric properties of BCT ceramics were systematically investigated to evaluate the suitability of $(Ba_{0.95}Ca_{0.05})TiO_3$ composite for electrical applications.

2 Materials and Methods

Specimens of the formula $(Ba_{0.95}Ca_{0.5})Tio_3$, were prepared according to the following firing technique. The starting materials ($BaCO_3$, TiO_2, $CaCO_3$) were 99.9% pure. Figure 1shown the block diagram of the solid-state reaction method. These components were weighted by

*Corresponding author E-mail: masoud.mostafa@sci.svu.edu.eg

stoichiometric ratios by using electronic analytical balances. The firing technique was performed in two successive stages. The first stage is called a first firing in which the component homogenized by grinding in an agate ball mill for 6 hours and then sifted and pressed into discs of 2 cm diameter and 1~ 1.5 cm thickness at 20 MPa. These pressed discs were calcined for 2 hours at a temperature between 1200 °C, 1400 °C according to the structure of the sample. The calcined powder was mixed with a very small amount of distilled water and pressed into discs at 40 MPa. The pressed disks were placed in a small silica crucible which was placed at the center of the big crucible and protected with aluminum oxide. The sintering temperatures (Ts) for the disks were 1400°C at sintering time (ts) equal to 2 hours. Finally, the disks were mechanically treated for producing samples with 7.5 mm diameter and about 1.5mm thickness and were coated with Aluminum thin film.

3 Results and Discussion

3.1 X-ray Diffraction

X-ray diffraction (XRD) was operated on the powders

using CuKα radiation at 40 kV and 25 A over the range 10–80° 2 θ. The powder XRD patterns were achieved from the powders calcined at 1200°C at a different temperate time using XRD (EMMA) GBC diffract meter in the range of Bragg's angle.

These patterns are shown in Figure 2 it is clear from the figure the case of the sample calcined at 1100°C, 1150°C, and 1200°C, the crystallization starts to form the perovskite BCT phase along but with small impurities of BO_2, Co_2, and TiO_2. The XRD patterns for the samples calcined at temperatures 1200°C also show that the perovskite phase is observed along with the BO_2 phase This indicates that Ca2+ ions were successfully incorporated into the BT lattices to form a homogeneous BCT single-phase powder [15].

From the XRD patterns, the crystal size was calculated by using Scherer's equation ($t = 0.9\lambda / \beta \cos\theta$) where λ is the wavelength of the x-ray, β is the full width at half-maximum (FWHM) and θ is the diffraction angle[16]. As shown in Fig. 2.

The refined XRD patterns of BCT ceramics the tetragonal strongest peak (1 1 0) and orthorhombic most solid peak (1 2 1). In Fig. 2. The (100) and (200) peaks splitting into (001) and (100), (002) and (200) indicates that all the prepared ceramics are tetragonal symmetry structure [17].
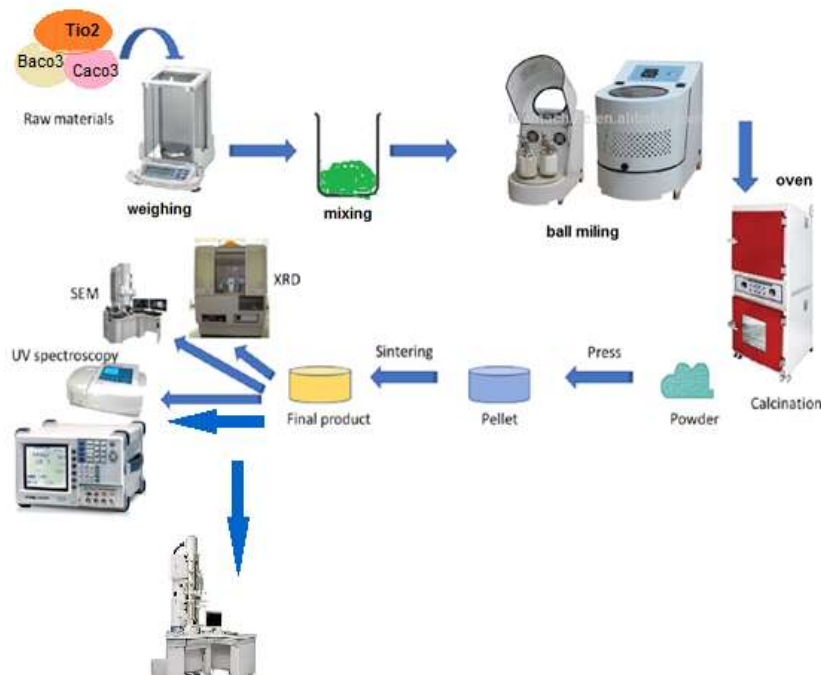

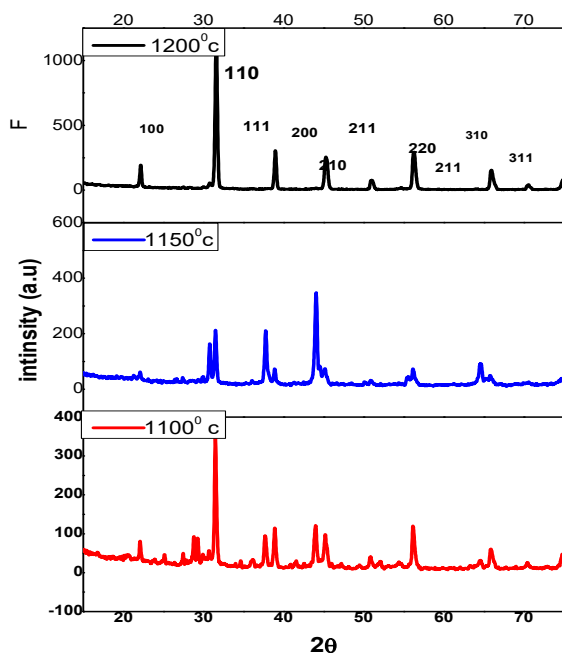**Fig. 1:** The block diagram of the solid-state reaction method.

3.2 Structure Refinements

Fig. 2: X-ray diffraction pattern of BCT powder, calcined at different temperatures.

the Rietveld refinement method utilized the atomic positions were determined from X-ray powder diffraction, and the Ti site was found to be associated with the Oxygen content. Least-squares structure refinements modeled with the FULLPROF Rietveld type program with conventional Rietveld R-factors for pattern, Rp = 76.5, the weighted pattern R factor (Rwp)= 69.7, and the expected R factor (Rexp) =29.82. Fig.3 shows a plot of the observed, calculated, and different profiles for the final Rietveld refinement for biogenically synthesized (Ba$_{0.95}$ Ca$_{0.05}$ Ti$_{1-x}$)O$_3$ nanoparticles (NPS). The agreement between the observations and the model during the evolution of the Rietveld refinements is indicated in the blue line in Figure 3. The analysis is performed by considering the space group as P4mm for the Tetragonal structure. A pseudo-Voigt function is applied to fit the several parameters of the XRD data. The refinement parameters such as occupancy, atomic functional position, crystal system, space group, cell parameter, cell volume of biogenically synthesized (Ba$_{0.95}$ Ca$_{0.05}$ Ti$_{1-x}$)O$_3$ nanoparticles (NPs) were determined and is tabulated in Table 2.
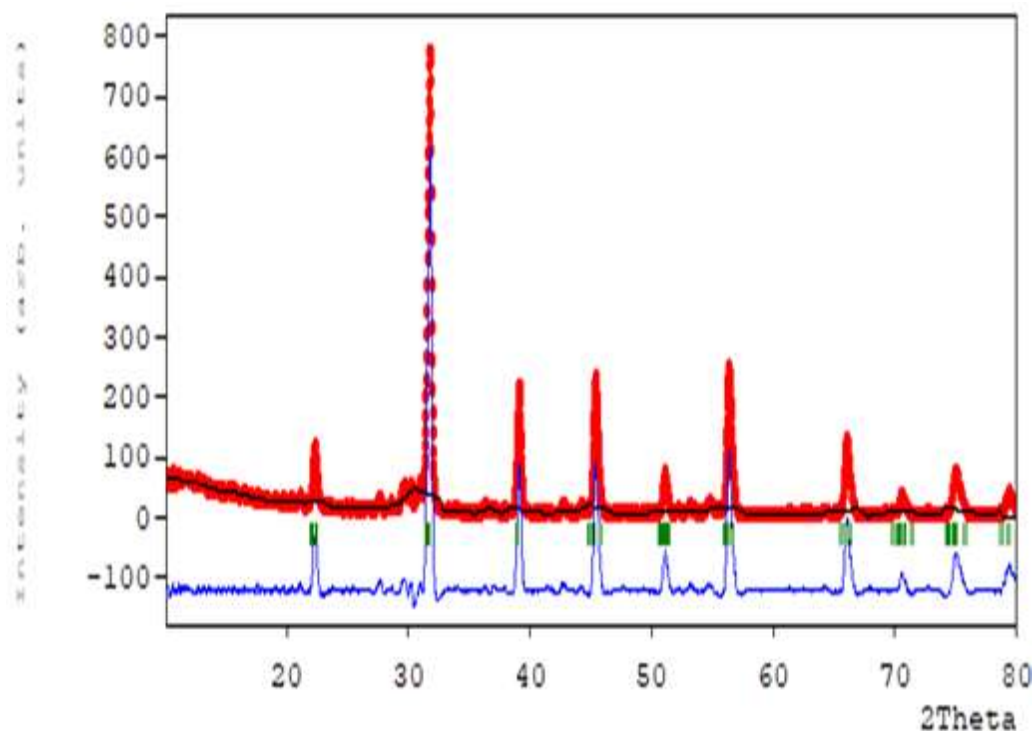

Fig.3: Rietveld refinement of Ba$_{1-x}$Ca$_x$TiO$_3$ samples with x = 0.05 using FullProf program.

Table 2: Final Rietveld refinement parameter of Tetragonal $(Ba_{0.95}Ca_{0.05}Ti_{1-x})O_3$ NPs.

Compound	Space group	a(Å)	b(Å)	c(Å)	α=β=γ	η=c/a	Cell volume(Å^3)	Atom	x	y	z
$(Ba_{0.95}Ca_{0.05}Ti_{1-x})O_3$	P4mm	3.95854	3.987283	4.00915	90°	1.012	62.8354	**Ba**	0	0	0
								Ca	0	0	0
								Ti	0.5	0.5	0.5
								O	0.5	0	0.5

The Final Rietveld refinement analysis for the XRD pattern cleared that $(Ba_{0.95}Ca_{0.05}Ti_{1-x})O_3$ Nps has a Tetragonal structure and highly crystalline.
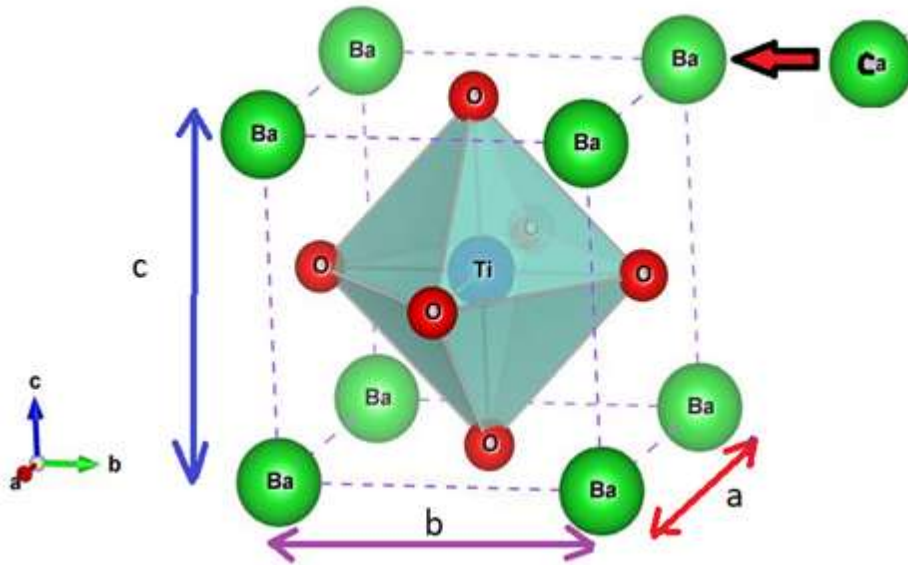
Fig.4: Schematic model of a $(Ba_{0.95}Ca_{0.05}Ti_{1-x})O_3$ structure with lattice constants a,b, and c.

The final Rietveld refinement parameters used in the standardization of crystal structure and fractional coordinates modeled by the VESTA (Visualization for Electronics and Structural Analysis) program[18], as shown in Fig.3. The crystal structure of $(Ba_{0.95}Ca_{0.05}Ti_{1-x})O_3$ NPs well-established to be *Tetragonal* corresponding to the space group P4mm. The *tetragonal* unit cell with three lattice parameters a,b, and c in the ratio of c/a = 1.012. A schematic representation of $(Ba_{0.95}Ca_{0.05}Ti_{1-x})O_3$ structure model using the final Rietveld refinement parameters is shown in Figure 4. The structure is composed of two interpenetrating Tetragonal sublattices.

3.3 SEM Analysis

Figure 5 shows the SEM micrographs pellets, the SEM micrograph was taken on the surface of the sample using the scanning electron microscope (SEM: JOEL JSM-5500 LV scanning microscope JEOL).

The samples were made the conducted from the thin layer of gold by using a sputter coater. the shape of the BCT (0.05 Ca) domain which was drawn on the micrograph of the pellet prepared from the BCT (0.05 Ca) powder. The SEM images of the obtained samples were processed with the ImageJ- Software [19] to determine the histogram for both the particle size and area. Aspherical morphology is observable, all particles are less than 6 μm. The particle sizes are in the range of 1– 6 μm. Particle size distribution histograms for BCT particle size and BCT particle area are presented in Figures 5(b) and 5(c), respectively. The average particle size of BCT has a larger average size in the range of 2– 3 μm, and the average area in the range 0.1– 0.12 μm^2.
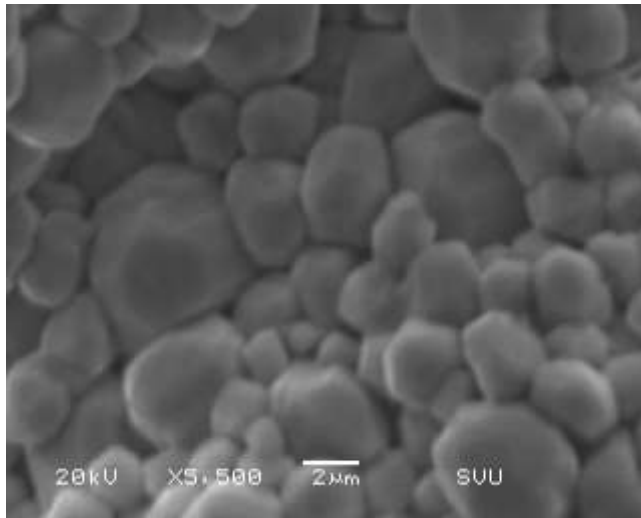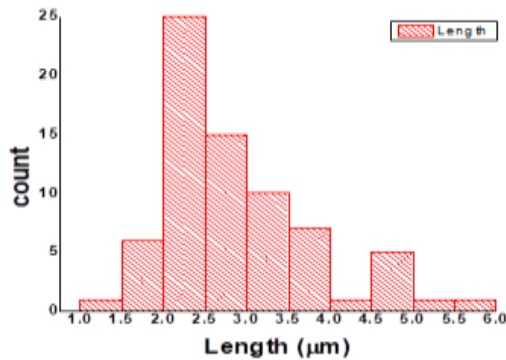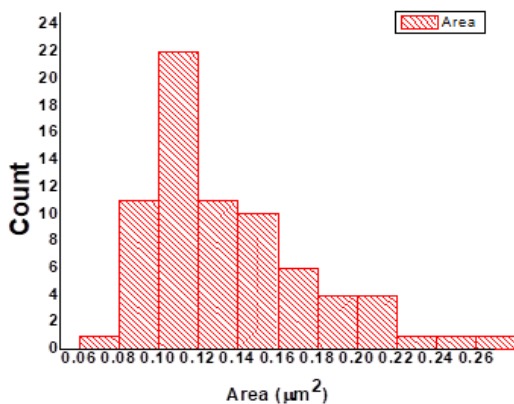
Fig.5(a): SEM images of BCT (0.05 Ca) ceramics sintered at 1400^0C .

(b)

(c)

Fig.5: SEM morphology (A) and the particle size distribution histogram (B) and the area distribution histogram (C).

3.4 TEM Analysis

Figure 6 presents the typical TEM images of the BCT powders doped with Ca 0.05% mol calcined at 1200^0C. According to TEM images.
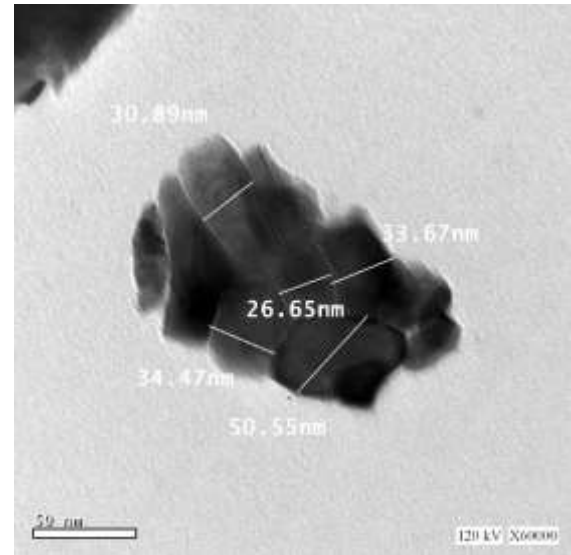

Fig.6: TEM images of BCT (0.05 Ca) ceramics.

As shown in TEM analysis, the primary crystallite size of the powder has been determined. The main particle size of the BCT (0.05 Ca) powder is approximately in the variety of 27–51 nm. From the TEM image, it is observed that the distribution of crystallite size of the powder is not uniform. It may be due to the agglomeration of crystallites caused during the preparation the powder of BCT (0.05 Ca) [20].

3.5 Optical Properties

Figure (7,8) shows the UV-V is Transmission spectra at room temperature, absorption spectra at room temperature presented in the same figure the wavelength for the spectrum of electrochemically synthesized in the range between 280 and 1200 nm.

Light with wavelengths in a range of approximately 200 to 400 nm is referred to as "UV", it is clear that the transmittance values increases rapidly in this range, but for light with wavelengths in a range of approximately 400 to 800 nm- which referred to as "visible light" increases slightly. For the range of approximately 800 to 1100 nm is referred to as "Near-Infrared", the transmittance decreases suddenly the increases again.   The energy gap was calculated for all samples with different calcined temperatures as shown in figure 9. The energy gap values agree with the literature for pure BCT. Figure 4 shows that the transmission values of BCT powder increase with the increasing wavelength, but the transmission curve for the Sn concentrations are changed.

G.M. Rashwan et al : Preparation and Characterization and …

The optical energy gap can be calculated using eq. (1) which is known as the Tauc plot [21].

$$h\alpha\gamma = (h\alpha\gamma - E_g^{opt})^2 \qquad (1)$$

Where h, γ, E_g^{opt} is the Plank constant, the frequency, optical energy gap, respectively and α is constant which equal the speed of the Light.

The values of the energy gap of pure $BaCa_{0.05}TiO_3$ as nanoparticles are in agreement with the literature [22]. The average calculated energy gap is approximately 5.2 eV.
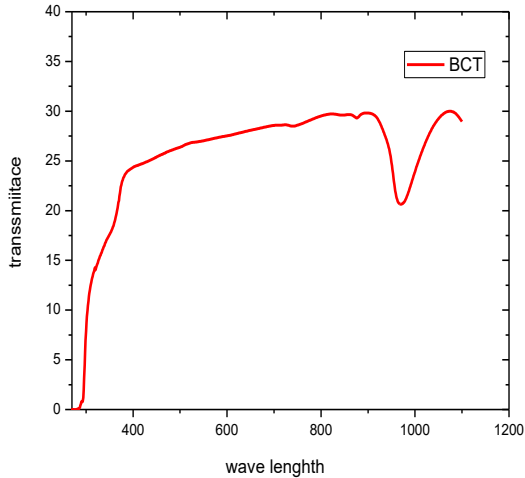

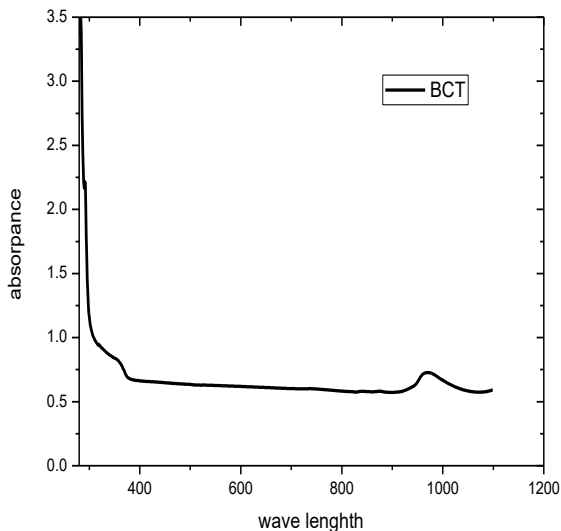**Fig. 7:** Transmittance spectra of BCT powders, calcined for 2h at 1200°C.

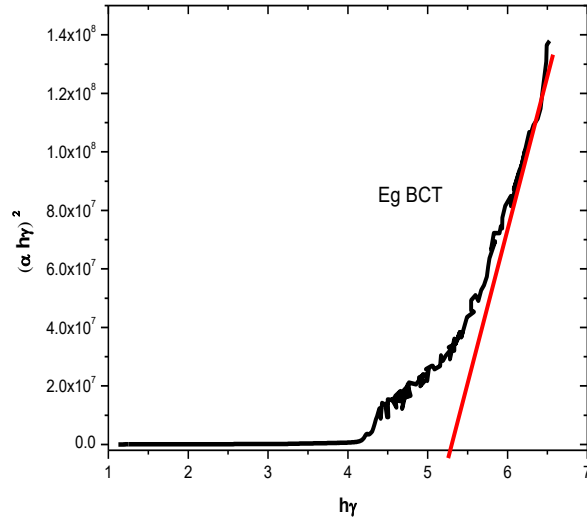**Fig. 8:** absorbance spectra of BCT powders, calcined for 2h at 1200°C.

Fig. 9: Energy gap of BCT powder, calcined for 2h at 1200 °C.

3.6 FT-IR Spectra

The Fourier-transform infrared spectroscopy (FT-IR) is obtained as transmission spectra of the KBr sample pellets to characterize the bond structure of the BCT nanoparticles. Fig. (10) shows the FT-IR of the BCT prepared by solid-state method calcined at 1200°c 2h sand sintering temperature 1400°c 3h in the range of 4000 – 400 cm^{-1}. Broadband near 657 cm^{-1}. According to the previous research about the titanate, this peak characterizes the vibration of the Ti-O octahedron [23]. This peak shift to a lower wavenumber at 550 cm^{-1} at sintering temperature 1400°c 3h [24], the two bands have been observed at 712cm-1 and 1004 cm^{-1} in the UV range. These bands were likely related to the stretching vibrations bonds C=O,

3.7 Dielectric Properties of BCT Nanoparticles

Figure 11 shows the relationship between the dielectric constant ε versus temperature for the same sample, which is characterized with the highest values of ε_{max},(1982) Also possesses the highest value of Debye's relaxation time. This result is important for saying the volume of the domain is proportional to Debye's relaxation time. This concussion is important for the interpretation of the results of dielectric properties for ferroelectric material based on critical Debye's relaxation time (τ_c). Figure (**12**) shows Debye's relaxation time (τ_c) of BCT is the highest relaxation time (τ_c) than other samples with a formula $(Ba_{0.95} Ca_{0.5)} TiO_3$; the relaxation time ($\tau_c$) for BCT is equaled to 1.77×10^{-5} sec.
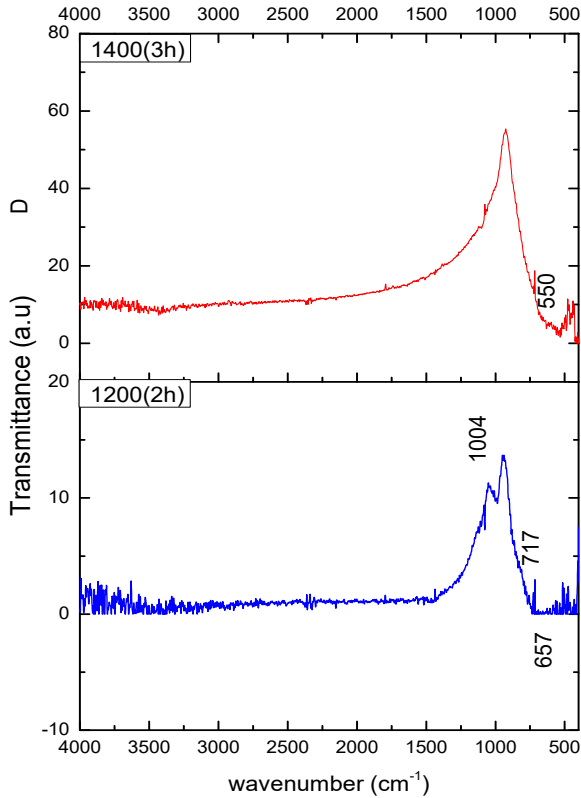
Fig.10:FT-IR spectra for (Ba0.95 Ca0.5)Tio3 nanoparticles calcined at 1200°c 2h sand sintering temperature 1400°c 3h.
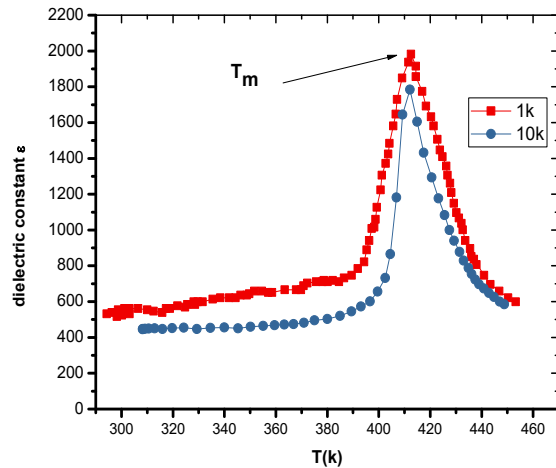

Fig. 11: Temperature dependence of the dielectric constant of BCT calcined at 1200°C and sintered at 1400°C for 2h.

Figure (13) shows that the behavior of the spontaneous polarization as a function of temperature, The general behavior is that the spontaneous polarization decrease with increasing temperature and it became zero at a temperature equal to Curie temperature, the maximum value of the

spontaneous polarization at Ca= 5 mol%, is equaled to 6.67×10^{-5} c/m^2

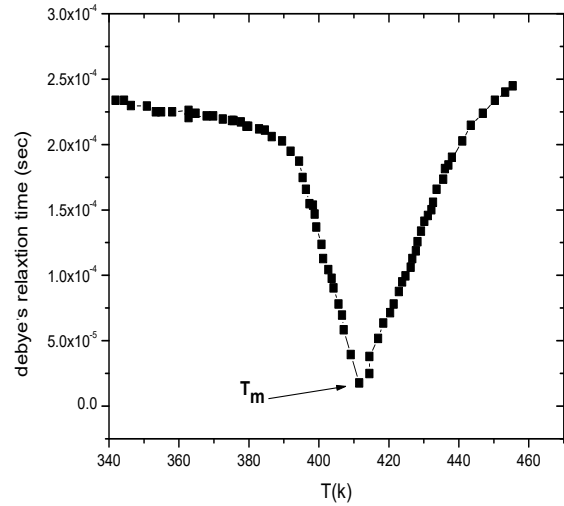**Fig.12:** Temperature dependence of the Debye's relaxation time of BCT calcined at 1200°C for 2 h, sintering at 1400°C.

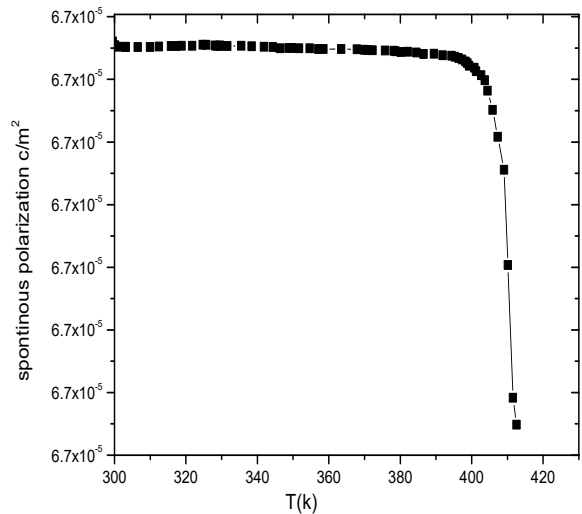**Fig.13:** Temperature dependence of spontaneous polarization of BCT calcined at 1200°C for 2 h, sintering at 1400°C.

The dielectric characteristics of a complex ferroelectric with diffuse phase transition can be explained by the Curie–Weiss law modified by Uchino and Nomura, where the diffuseness degree of the phase transition can be calculated as:

$$\frac{1}{\varepsilon - \varepsilon m} = \frac{(T - Tm)\gamma}{C}$$

Where $\mathcal{E}$ is the dielectric permittivity corresponding to T, $\mathcal{E}_m$ is the maximum dielectric constant corresponding to Curie temperature T_m, C is the Curie constant, and c represents the diffused phase The magnitude of $\gamma= 1$ represents that the material belongs to a normal ferroelectric and the normal Curie–Weiss law is obtained. Thus, $1> \gamma> 2$ indicates that the material belongs to a relaxer ferroelectric and the material exhibits diffuse phase transition with a broad permittivity temperature curve (figure 14). The value of $\gamma= 2$ represents an ideal ferroelectric relaxer and describes a completely diffuse phase transition [25], [26].
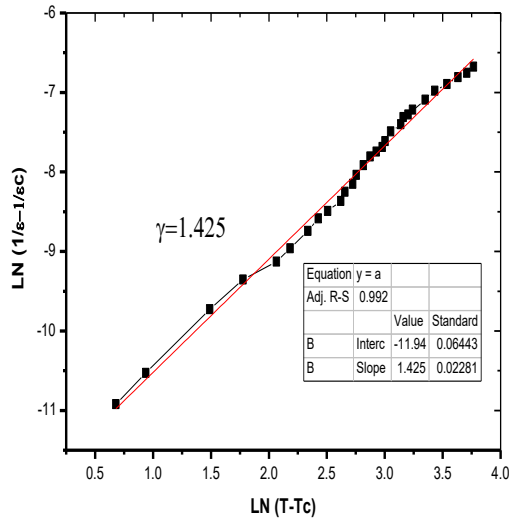

Equation	y = a	
Adj. R-S	0.992	
		Value	Standard
B	Interc	-11.94	0.06443
B	Slope	1.425	0.02281

$\gamma=1.425$

Fig.14: Temperature dependence of Curie–Weiss of BCT.

4 Conclusions

Initially the discovery of the high dielectric constant and later that the discovery of the enhancement of the dielectric constant by the ferroelectricity of barium titanate ceramics led to the utilization of ABO_3 crystals as ferroelectrics. The electrical poling of barium titanate provided the complete alignment of all the domains in the ceramic as in the single crystals. The relatively low Curie temperature (120°C) of barium titanate restricts its usage in MEMS applications. From XRD observation, crystallographic information about a tetragonal distortion of BCT crystal was identified. According to these results, it might be due to BCT ceramics transformed from the tetragonal phase to
cubic phase, SEM micrograph was taken on the surface of the sample using the scanning electron microscope, the dielectric constant ε with temperature for the same sample, which is characterized with highest values of ε_{max} equal to(1982) Also possesses the highest value of Debye's relaxation time$1.77x10^{-5}$ sec and the spontaneous polarization as a function of temperature $6.67x10^{-5}$ c/m^2

Declarations
Author contribution statement

References

[1] L. B. Kong, S. Li, T. S. Zhang, J. W. Zhai, F. Y. C. Boey, and J. Ma, "Electrically tunable dielectric materials and strategies to improve their performances," Prog. Mater. Sci., **55(8)**, 840–893, 2010, doi: 10.1016/j.pmatsci.2010.04.004.

[2] X. X. Xi et al., "Oxide thin films for tunable microwave devices," J. Electroceramics., **4(2)**, 393–405, 2000, doi: 10.1023/a:1009903802688.

[3] A. Priya, E. Sinha, and S. K. Rout, "Structural, optical and microwave dielectric properties of BaS_xSrxWO4 ceramics prepared by solid state reaction route," Solid State Sci., **20**, 40–45, 2013.

[4] B. M. Patil, R. S. Srinivasa, and S. R. Dharwadkar, "Synthesis of CaTiO3 from calcium titanyl oxalate hexahydrate (CTO) as precursor employing microwave heating technique," Bull. Mater. Sci., **30(3)**, 225–229, Jun. 2007, doi: 10.1007/s12034-007-0040-7.

[5] M. J. Gázquez, J. P. Bolívar, R. Garcia-tenorio, and F. Vaca, "A Review of the Production Cycle of Titanium Dioxide Pigment.,". **May**, 441–458, 2014.

[6] H.-C. Li, W. Si, A. D. West, and X. X. Xi, "Near single crystal-level dielectric loss and nonlinearity in pulsed laser deposited SrTiO3 thin films," Appl. Phys. Lett., **73(2)**, 190–192, Jul. 1998, doi: 10.1063/1.121751.

[7] A. Outzourhit, J. U. Trefny, T. Kito, and B. Yarar, "Tunability of the dielectric constant of Ba0.1Sr0.9TiO3 ceramics in the paraelectric state," J. Mater. Res., vol. 10, no. 6, pp. 1411–1417, 1995, doi: DOI: 10.1557/JMR.1995.1411.

[8] W. Chang and L. Sengupta, "MgO-mixed Ba0.6Sr0.4TiO3 bulk ceramics and thin films for tunable microwave applications," J. Appl. Phys., **92(7)**, 3941–3946, 2002, doi: 10.1063/1.1505669.

[9] M. W. Cole, P. C. Joshi, and M. H. Ervin, "La doped Ba1−xSrxTiO3 thin films for tunable device applications," J. Appl. Phys., **89(11)**, 6336–6340, Jun. 2001, doi: 10.1063/1.1366656.

[10] O. A. Ramdasi, S. G. Kakade, R. C. Kambale, and Y. D. Kolekar, "Ferroelectric and Dielectric Properties of BT based Lead Free Ceramics," Res. J. Mater. Sci., **4(3)**, 7–9, 2016.

[11] L. Y. Li and X. G. Tang, "Effect of electric field on the dielectric properties and ferroelectric phase transition of sol-gel derived (Ba0.90Ca0.10)TiO3 ceramics," Mater. Chem. Phys.,**115(2–3)**,507–511,2009,doi: 10.1016/j.matchemphys.2009.01.023.

[12] Q. Yue, L. Luo, X. Jiang, W. Li, and J. Zhou, "Aging effect of Mn-doped Ba0.77Ca0.23TiO3 ceramics," J. Alloys Compd.,**610**,276–280,2014,doi: 10.1016/j.jallcom.2014.05.003.

[13] X. Cheng and M. Shen, "Different microstructure and dielectric properties of Ba1-xCaxTiO3 ceramics and pulsed-laser-ablated films," Mater. Res. Bull., **42(9)**, 1662–1668, 2007, doi: 10.1016/j.materresbull.2006.11.033.

[14] M. R. Panigrahi and S. Panigrahi, "Synthesis and microstructure of Ca-doped BaTiO3 ceramics prepared by high-energy ball-milling," Phys. B Condens. Matter., **40(21)**, 4267–4272, 2009, doi: 10.1016/j.physb.2009.08.012.

[15] Q. Zhang, J. Zhai, Q. Ben, X. Yu, and X. Yao, "Enhanced microwave dielectric properties of Ba0.4Sr0.6TiO3 ceramics doping by metal Fe powders," J. Appl. Phys., **112(10)**, 104104, Nov. 2012, doi: 10.1063/1.4766276.

[16] M. Mostafa, K. Ebnalwaled, H. A. Saied, and R. Roshdy, "Effect of laser beam on structural, optical, and electrical properties of BaTiO3 nanoparticles during sol-gel preparation," J. Korean Ceram. Soc., **55(6)**, 581–589, 2018, doi: 10.4191/kcers.2018.55.6.04.

[17] A. H. Dent, A. Patel, J. Gutleber, E. Tormey, S. Sampath, and H. Herman, "High velocity oxy-fuel and plasma deposition of BaTiO3 and (Ba,Sr)TiO3," Mater. Sci. Eng. B Solid-State Mater. Adv. Technol., **87(1)**, 23–30, 2001, doi: 10.1016/S0921-5107(01)00653-5.

[18] K. Momma and F. Izumi, "{\it VESTA3} for three-dimensional visualization of crystal, volumetric and morphology data," J. Appl. Crystallogr., **44(6)**, 1272–1276, 2011, doi: 10.1107/S0021889811038970.

[19] M. D. Abràmoff, P. J. Magalhães, and S. J. Ram, "Image processing with imageJ," Biophotonics Int., **11(7)**, 36–41, 2004, doi: 10.1201/9781420005615.ax4.

[20] G. M. R. M.K. Gerges, M. Mostafa, "Structural, optical and electrical properties of PbTiO3 nanoparticles prepared by Sol-Gel method," Ijlret., **2(4)**, 42–49, 2016.

[21] J. Tauc, "Optical Properties of Amorphous Semiconductors BT - Amorphous and Liquid Semiconductors," J. Tauc, Ed. Boston, MA: Springer US., 1974, 159–220.

[22] S. Piskunov, E. Heifets, R. I. Eglitis, and G. Borstel, "Bulk properties and electronic structure of SrTiO3, BaTiO 3, PbTiO3 perovskites: An ab initio HF/DFT study," Comput. Mater. Sci., **29(2),** 165–178, 2004, doi: 10.1016/j.commatsci.2003.08.036.

[23] Sun, Dazhi, et al. "Investigation on FTIR spectrum of barium titanate ceramics doped with alkali ions." Ferroelectrics **355(1)**, 145-148, 2007.

[24] Aal, A. Abdel, et al. "FTIR study of nanostructure perovskite BaTiO3 doped with both Fe3+ and Ni2+ ions prepared by sol-gel technique." Acta Phys. Pol., **A 126.6**, 1318-1322, 2014.

[25] L. Cui, Y.-D. Hou, S. Wang, C. Wang, and M.-K. Zhu, "Relaxor behavior of (Ba,Bi)(Ti,Al)O3 ferroelectric ceramic," J. Appl. Phys., **107(5)**, 54105, 2010, doi: 10.1063/1.3327244.

[26] M. Mostafa, Z. A. Alrowaili, G. M. Rashwan, and M. K. Gerges, "Ferroelectric behavior and spectroscopic properties of La-Modified lead titanate nanoparticles prepared by a sol-gelmethod,"Heliyon.,**6(2)**,2020,doi: 10.1016/j.heliyon.2020.e03389.